Optical Materials: X 16 (2022) 100205

Contents lists available at ScienceDirect

Optical Materials: X

journal homepage: www.journals.elsevier.com/optical-materials-x

(INVITED)Direct laser writing of visible and near infrared 3D luminescence patterns in glass

Fouad Alassani [a,*], Gustavo Galleani [b], Guillaume Raffy [c], André Del Guerzo [c], Arnaud Royon [d], Kevin Bourhis [d], Andrea Simone Stucchi de Camargo [b], Véronique Jubera [a], Lionel Canioni [e], Thierry Cardinal [a], Yannick Petit [a,e]

[a] Université de Bordeaux, CNRS, Bordeaux INP, ICMCB, UMR 5026, F-33600, Pessac, France
[b] Physics, University of São Paulo, Av. Trabalhador Sãocarlense 400, São Carlos, 13566-590, SP, Brazil
[c] Université de Bordeaux, CNRS, Institute of Molecular Sciences (ISM, UMR 5255), F-33400, Talence, France
[d] Argolight SA, Cité de Photonique, 33600, Pessac, France
[e] Université de Bordeaux, CNRS, CEA, CELIA, UMR 5107, F-33405, Talence, France

ARTICLE INFO

Keywords:
Femtosecond laser writing
Silver cluster
Energy transfer
3D near IR luminescence
Co-localized silver clusters
And ytterbium ions

ABSTRACT

We report the fluorescent properties of 3D localized structure with size near the diffraction limit induced by femtosecond direct laser writing (DLW) in Yb^{3+} and silver-containing phosphate glass. The homogenous dispersion of the silver ions and Yb^{3+} ions in the glass matrix before DLW was evidenced using photoluminescent spectroscopy and time-resolved spectroscopy. Using high repetition rate femtosecond DLW, the inscription of 3D visible and near-infrared fluorescent patterns formed by co-localization of silver cluster and Yb^{3+} ions was demonstrated. The local refractive index change associated with the formation of silver clusters is dependent on the laser irradiance. Confocal micro-luminescent spectroscopy for excitation wavelength in the visible range shows efficient emission of Yb^{3+} only on DLW induced 3D fluorescent patterns. This finding demonstrated the ability to perform thanks to DLW laser a resonant efficient nonradiative energy transfer from silver clusters to Yb^{3+} and allows 3D writing of near-infrared luminescence.

1. Introduction

The Femtosecond (fs) Direct Laser Writing (DLW) technique plays a major role as a flexible, fast, cost-effective, highly transferable approach to industrial processes, it enables highly-integrated optical functionalities and photonic integrated circuits (PIC) [1]. Nowadays, there is a growing demand for developing all-optical approaches to create 3D multi-scale architectures including sub-wavelength dimensions for application in different sectors of the economy such as in the market of sensors. Recently, we have developed new expertise in fabricating multi-scale photonic architectures using all-optical fs laser writing in specialty-designed photosensitive silver-containing glasses [2]. One of the challenges relies on the capability of structuring the local luminescent properties. Femtosecond DLW in silver-containing glasses allows for the local creation of an elementary brick with inner features below the diffraction limit, possibly down to 100 nm [3]. Such a modification is due to highly luminescent silver clusters formed by local aggregation of silver atoms and silver ions, which result from the laser-activated migration and chemical reactivity of the silver ions in the glass matrix. Such laser-induced molecular species emit in the whole visible range upon excitations from 270 nm up to 530 nm. It clearly appears that the all-optical structuring is highly dependent on the glass host, the silver species environment in the pristine glass, and the DLW parameters [4,5]. The co-doping of silver ions with other noble metal ions or rare earth elements and their interaction in order to tune the luminescence properties from the ultraviolet (UV) to the near infra-red (NIR) range has been widely reported by various groups in several glass matrix [6–10]. Many applications for optoelectronic devices such as white light emitting diodes, three-dimensional (3D) displays, and efficiency enhancement of solar cells have been demonstrated [7,9–12]. Since the discovery of the enhancement of the europium ions emission in silver-containing glass by Malta et al. [10], many investigations of the interaction between silver nanoparticles or silver clusters and other noble metals or rare earth ions have triggered attention [7–10]. Indeed

* Corresponding author.
E-mail address: fouad.alassani@u-bordeaux.fr (F. Alassani).

https://doi.org/10.1016/j.omx.2022.100205
Received 26 August 2022; Received in revised form 16 October 2022; Accepted 19 October 2022
Available online 16 November 2022

the preparation method of the glass matrix containing both silver and rare earth ions by means of conventional melt-quenching or ion exchange techniques favors the formation of silver nanoclusters or nanoparticles randomly distributed in the sample's volume, which can modulate the luminescence properties of the rare earth ion either by energy transfer or by local field effect induced by surface plasmon resonance [10,13–15]. Different studies have been devoted to bulk homogeneous samples. The 3D architecting of rare earth luminescence properties remains a challenge. Recently, we demonstrated in Eu^{3+} doped silver-containing phosphate glasses the possibility to influence the emission spectrum of Eu^{3+} ions thanks to the production of laser-inscribed highly-localized 3D fluorescence structures of silver clusters with high optical contrast [4]. The photo-induced silver clusters exhibiting high absorption intensity starting from the UV until 530 nm, undergo resonant energy transfer to the Eu^{3+} ions, allowing the obtainment of tunable, localized, and high-contrast luminescence over the visible range.

In this work, we report on the intrinsic luminescence properties of Yb^{3+} in a silver-containing phosphate glass (labeled PZn:Ag–Yb), the creation of molecular silver clusters in the presence of Yb^{3+} ions, as well as the efficient non-radiative energy transfer mechanism operating from 3D localized silver clusters towards the neighboring Yb^{3+} ions. The results evidence direct experimental access to 3D-localized multi-scale background-free Yb^{3+} IR emission with excitation that can be totally mediated through the excitation of laser-inscribed silver clusters.

2. Experimental section

2.1. Glass synthesis and sample preparation

The synthesis of Yb^{3+} doped silver-containing phosphate glass samples in the compositional system (100-x)[40$PO_{5/2}$-55ZnO-1$GaO_{3/2}$-4$AgO_{1/2}$] − xYb_2O_3 (mol. %), x ranging from 0 to 2, has been performed using H_3PO_4 (Roth, 85%), Na_2CO_3 (Alfa Aesar, 99.95%), Ga_2O_3 (Strem Chemicals, 99.998%) and $AgNO_3$ (Alfa Aesar, 99.995%) and Yb_2O_3 (Sigma-Aldrich, 99.9%) precursors. All the precursors were homogeneously mixed in a Teflon beaker in an aqueous solution and dried on the sand bath for 12 h to obtain cement. The cement was then ground and introduced in a platinum crucible and melted a 1250°C for 10 h. The melt was quenched at room temperature to obtain the final glass samples. The obtained glasses were annealed at 40°C below the T_g for 4 h to reduce mechanical strength induced during the quenching. Then, the glasses were cut into small slices (1 mm thick) and optically polished on the two faces for optical quality. Table 1 presents the label and the theoretical composition of the studied samples.

2.2. Pristine glass characterization

UV–Visible transmission spectroscopy has been performed on the pristine glass using a Cary 5000 spectrophotometer in the range of 250–2000 nm with a step of 0.2 nm and integration time of 0.1 s.

The infrared transmission spectra were recorded on a spectrometer Brüker Equinox 55 from 4000 cm^{-1} to 1000 cm^{-1} with a spectral resolution of 4 cm^{-1} and purged with dry air before measurement.

The excitation and emission spectroscopies were performed at room temperature with both a SPEX Jobin Yvon fluorescence spectrometer equipped with a double monochromator, a UV grating blazed at 350 and Peltier cooled PMT (Horiba Jobin Yvon Gmbh, Haching, Germany) for the UV spectrum range. For the near-infrared range, Fluorolog-3 spectrofluorimeter (Horiba Jobin-Yvon) equipped with an InGaAs detector, cooled with liquid nitrogen and a grating blazed at 600 was used. The excitation source of both spectrometers was a Xenon lamp enabling continuous excitation from 200 to 800 nm and the collected spectra data were corrected from both the spectral lamps distribution and the detector sensitivity. An abb-refractometer enabling a precision of ±0.002 was used to determine the refractive index of the glasses at 589 nm.

Table 1
Sample compositions.

Glass samples	Compositions (Theoretical mol. %)					
	P_2O_5	ZnO	Ga_2O_3	Ag_2O	Na_2O	Yb_2O_3
PZn:Ag	40	55	1	4		
PZn:Ag-0.25 Yb	39.7	55	1	4		0.25
PZn:Ag-2Yb	39	54	1	4		2
PZn:Na-2Yb	39	54	1		4	2

Yb^{3+} lifetime measurements were performed with a digital oscilloscope (LeCroy Waverunner LT 342) equipped with a germanium AD403HS detector coupled to an HR640 monochromator (Horiba Jobin-Yvon). A self-made Labview program was used for piloting the experiments.

2.3. Femtosecond direct laser writing (DLW)

The femtosecond (fs) DLW was performed with a Ytterbium fs oscillator (up to 2.6 W, 9.1 MHz, and 390 fs FWHM at 1030 nm). To control the transmitted irradiance, the system is combined with an acousto-optic modulator, allowing to focus of both the energy and the irradiance up to 100 nJ and 20 $TW.cm^{-2}$ respectively. A high-precision XMS-50 translation stage, enabling a precision of up to 50 nm was used to position and displace the sample during DLW irradiation. Zeiss microscope objective (20 × , 0.75 NA) was used to generate the DLW structure at 160 μm below the sample surface. To eliminate spherical aberrations, a spatial light modulator (LCOS; X10468-03, Hamamatsu Photonics) was used. The glass sample was moved using a three-coordinate motorized magnetic-levitation translation stage (Newport) synchronized with the laser. The irradiance is described by the following equation:

I_peak = (mean power/repetition rate)/[mean pulse duration x mean pulse focused section]

2.4. Refractive index change

The refractive index change (Δn) between the pristine glass and the DLW's structures was measured using a phase-contrast microscopy method with commercially available wave-front sensor SID4Bio from PHASICS. White light and a 100 × – 1.3 NA oil immersion objective were used to image the structure.

2.5. Fluorescence micro-spectroscopy of the structured sample

The Fluorescence spectrum measurements of DLW's structures were performed using a high spectral resolution micro-spectrometer (LabRAM HR800 from Jobin-Yvon, Horiba Jobin Yvon GmbH, Haching, Germany) with a 300 grooves.cm^{-1} grating, equipped with liquid nitrogen cooled InGaAs detector, for the spectral dispersion of the fluorescence in the near-infrared range at three different excitation wavelength (325 nm, 405 nm and, 532 nm). The 325 nm excitation was performed with a UV He–Cd laser source (30 mW, TEM 00, Kimmon, Tokyo, Japan) using a focused UV-enhanced Cassegrain objective (36 × , NA 0.5) in order to limit the refractive index dispersion effect on the measurement. The 405 nm and 532 nm excitation were performed with a near-UV laser diode (100 mW, TEM00, OBIS from COHERENT, Santa Clara, CA, USA) and a laser diode (100 mW, TEM00, monomode, Coherent, Santa Clara, CA, USA) respectively. An Olympus refractive objective (50 × , NA 0.9) was used for the latter with two excitation wavelengths. The fluorescence spectra for the three conditions were collected over the range of 900 – 1100 nm.

2.6. Fluorescence hyper-spectral micro-imaging of the structured sample

The fluorescence hyper-spectral micro-imaging was performed using

a Picoquant MT200 microscope equipped with a spectrometer and a CCD camera, which allows for the recording of the full emission spectrum over the visible range up to the near-IR detection limit of the detector. Excitation was achieved with a CW laser diode source at 473 nm. The visible and near-IR micro-images of the laser-inscribed patterns resulted from the spectral integrations over the 500–700 nm and 920–1050 nm spectral ranges, respectively.

3. Results and discussions

3.1. Absorption spectroscopy

Fig. 1 shows the absorption spectrum covering the UV/Visible/mid-IR spectrum range of Yb^{3+} doped silver-containing and silver-free zinc phosphate glasses having different molar concentrations of Yb^{3+}: 0.25% (black curve) and 2% (red and blue curves). The absorption band ranging from 900 to 1050 nm with a maximum at 975 nm (Fig. 1b) is characteristic of the $^2F_{7/2} \rightarrow {}^2F_{5/2}$ transitions of Yb^{3+}. The full width half maximum, typically spanning from before 900 nm up to more than 1025 nm, reflects the global splitting of the $^2F_{5/2}$ excited state by the crystal field effect if we consider that the absorption occurs from the lowest stark component of the $^2F_{7/2}$ ground state neglecting the absorption from the upper component. The PZn:Ag and PZn:Na-2Yb samples were used as references to obtain the pure signal of silver ions and Yb^{3+} respectively. The absorption coefficients of Yb^{3+} in the glasses containing 2% of Yb^{3+} are quite similar, which reveals a non-relevant competition of absorption between silver ions and Yb^{3+} in the NIR range. However, the absorption coefficient of Yb^{3+} in the silver-containing zinc phosphate glass doped with 0.25% of Yb^{3+} is almost 8 times lower than those containing 2% of Yb^{3+}which is in a good correlation with the ratio of the estimated number of Yb^{3+} per volume illustrated in Table 2. The absorption edge in the UV range of the sample containing both silver and Yb^{3+} is shifted to the red side as compared to the sample containing only Yb^{3+} (Fig. 1a). This effect results from the presence of silver ions which present a strong absorption between 200 nm and 300 nm [16]. Above 300 nm no additional absorption is observed, thus no evidence of a plasmonic effect. Furthermore, absorption spectra have been measured in the mid-IR range where hydroxyl groups are responsible for a broad feature, as shown in Fig. 1c. One can observe that the maximum absorption coefficient of OH in glasses containing 2% of Yb^{3+} is lower than that for the glass containing 0.25% of Yb^{3+}. To elucidate this effect of decreasing intensity of the OH absorption band with Yb^{3+}, we have performed the calculation of OH content per volume using reference data from silica glass [17] and extrapolated to phosphate glass (see table Table 1). It shows that the glass containing the highest concentration of Yb^{3+} presents the lowest OH^- content (a reduction of about 28%). This indicates that Yb^{3+} not only behaves as a dopant but also as a reticulation agent of the glass network, preventing the formation of P–O–H groups.

Table 2
Concentration of Yb^{3+} and Ag^+ ions in the PZn glasses from the theoretical glass compositions presented in table1.

Samples	Number of Ag^+ ions (per cm^3)	Number of Yb^{3+} ions (per cm^3)	Cross section of Yb^{3+} ions at 975 nm (cm^2)	Number of OH (per cm^3)
PZn:Ag-0.25 Yb	10.179×10^{20}	0.638×10^{20}	1.95×10^{-20}	12.63×10^{19}
PZn:Ag-2Yb	9.902×10^{20}	5.056×10^{20}	2.06×10^{-20}	8.97×10^{19}
PZn:Na-2Yb	10.038×10^{20}	5.126×10^{20}	2.21×10^{-20}	9.36×10^{19}

3.2. Photoluminescence properties of Yb^{3+} and silver ions

The luminescence spectroscopy of the silver and/or Yb^{3+} containing Zinc phosphate glass samples was performed. Fig; 2 illustrated the corresponding excitation and emission spectrum of silver ions and Yb^{3+} in the phosphate matrix. The distribution of silver ions depending on the presence of Yb^{3+} has been investigated by photoluminescence spectroscopy. Fig; 2a presents the excitation and the emission spectra of PZn:Ag, PZn:Ag-0.25 Yb and PZn:Ag-2Yb glasses. For PZn:Ag and PZn:Ag-0.25 Yb glasses, the excitation at 230 nm induces two broad emission bands with maximum respectively at 280 nm and 370 nm. These emission bands are characteristic of different environments of silver ions named site A (isolated silver ions Ag^+) and Site B (silver pairs Ag^+-Ag^+) [3,5]. In the PZn:Ag-2Yb glass sample, a decrease in emission of site A emission as compared to that of site B is observed. Since such a phenomenon is observed for excitation at 230 nm, this can be related to the reabsorption of the emission of isolated silver ions by the tail of the charge transfer band of Yb^{3+} or to a change in the proportion of site A with respect to site B in Yb^{3+}-doped sample. To evaluate the effect of Yb^{3+} ions on the distribution of site B, excitation and emission spectra were recorded at the longest wavelength and are presented in Fig. 2b. The B site emission spectrum is quite similar for all samples, one can notice only a slight red shift of the excitation band for PZn:Ag-2Yb glass. Thus, one can suspect that the introduction of 2% of Yb^{3+} tends to decrease the contribution of site A leading to an increase in the relative intensity of the site B emission. The introduction of Yb^{3+} then slightly affects the distribution of silver ions.

The emission spectrum of Yb^{3+} in the near infrared for the excitation at 260 nm of the PZn:Ag-2Yb and PZn:Na-2Yb glasses are presented in Fig. 2c. The UV wavelength corresponds to an excitation in the charge transfer band of the Yb^{3+} ions. Because of the very high associated

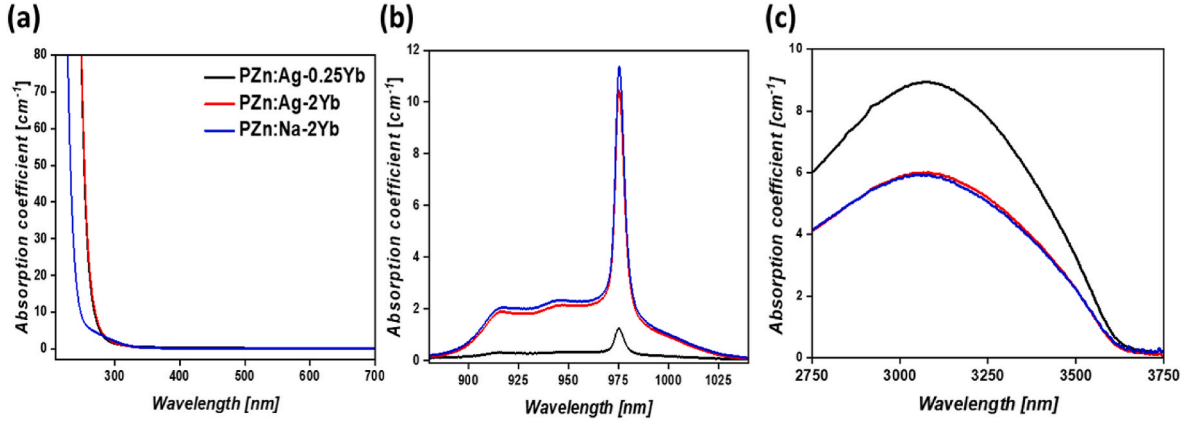

Fig. 1. Absorption spectra of Yb^{3+}-doped and Yb^{3+}-free silver containing PZn pristine glass. (a) Absorption edge in UV range; (b) Absorption band of Yb^{3+}; (c) Absorption band of P–OH.

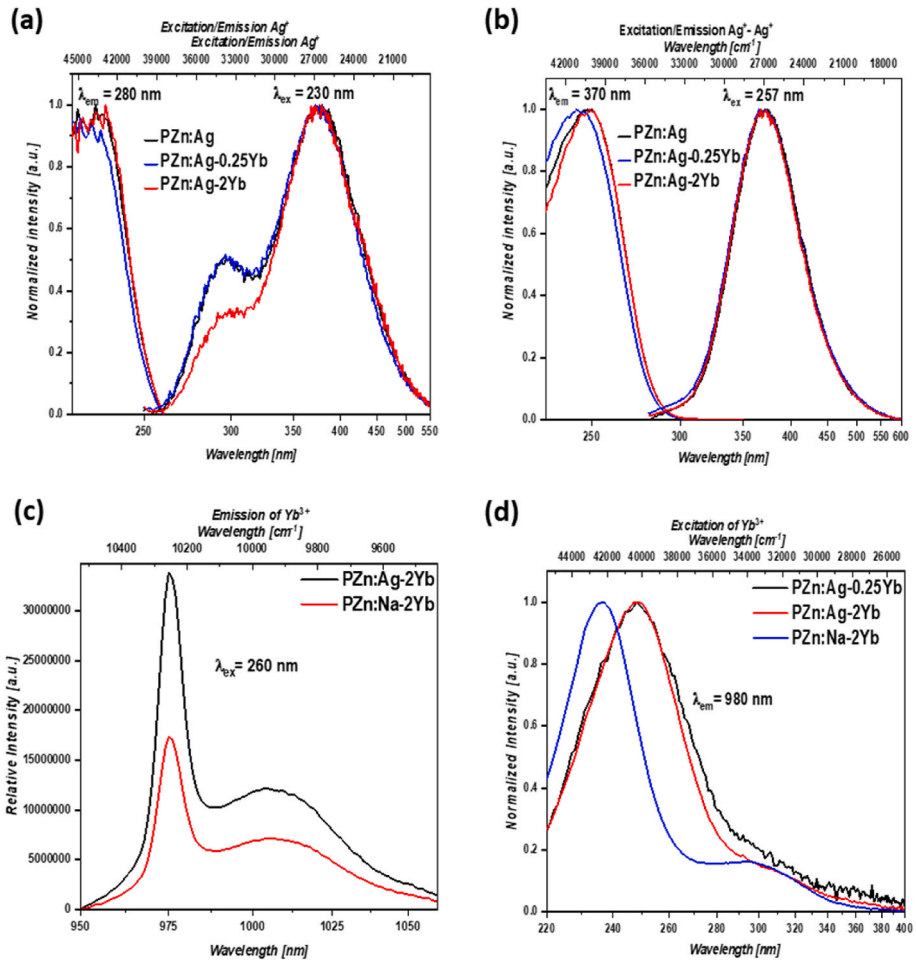

Fig. 2. Excitation and emission spectra of Ytterbium doped and undoped PZn4Ag glass. (a) Excitation/emission spectra of Ag^{+} ions; (b) Excitation/emission spectra of Ag^{+}- Ag^{+}; (c) emission spectrum of Yb^{3+} ions for 260 nm excitation; (d) Excitation spectrum of Yb^{3+} ions for 980 nm emission.

absorption coefficient (see Fig. 1), absorption occurs within a very limited penetration depth, namely most likely at the surface of the crushed glass grains being used for this measurements. As a consequence, the fluorescence emission mostly comes directly from the surface of these crushed grains, so that the emitted photons have undergone a limited propagation within the bulk of these glasses. In such conditions, it can be expected that reabsorption phenomena can be neglected compared to cases such as bulk excitation with the near-IR 4f-4f absorption transitions. Therefore, the corresponding observed emission spectra are expected not be distorted by partial attenuation due to reabsorption of the most energetic emission wavelengths (the "blue" part of the Yb^{3+} emission spectrum), compared to the least energetic ones (the "red" part of the Yb^{3+} emission spectrum). The spectra exhibit a broad emission band ranging from 900 nm to 1050 nm range with a sharp peak around 975 nm. The most intense band at 975 nm is assigned to the radiative transition from the lowest stark sublevel of $^{2}F_{5/2}$ level to lowest stark sublevel of $^{2}F_{7/2}$ levels (such transition being usually referred to as the zero phonon line) [18]. The amplitude of the emission band of Yb^{3+} is two times higher in silver containing glass than in silver free glass. This phenomenon suggests that there is an energy transfer mechanism from Ag^{+} ions to Yb^{3+} ions. Indeed, 260 nm excitation wavelength can promote an emission of silver species (discussed in the following paragraph), which can transfer part of the emission energy to the closest Yb^{3+} ions, resulting in efficient emission of Yb^{3+}. The same phenomenon has been observed, not only in oxyfluoride phosphate glass co-doped Ag^{+}-Yb^{3+} but also in phosphate glass co-doped silver and other rare earth elements [4,6,19,20]. The excitation spectra for the 980 nm emission have been measured and are presented in Fig. 2b. For PZn: Na–Yb glass, two broad excitation bands are observed. The most intense component with a maximum recorded at 235 nm is attributed to the charge transfer excitation from O^{2-} coordinating anions of the host matrix to the central Yb^{3+} ions [6]. However, the origin of the less intense band centering around 300 nm, which is not a usual charge transfer band of Yb^{3+}, is probably due to impurities in the glass. For PZn: Ag-0.25 Yb and PZn:Ag-2Yb glasses, the excitation spectrum exhibits a broad band covering the whole UV region, with a maximum around 250 nm. This broad band originates from the superposition of several bands such as the excitation band of silver ions with a maximum around 250 nm, and O^{2-}→Yb^{3+} charge transfer excitation band observed in the silver free glass.

3.3. *Time resolved spectroscopy of the Yb^{3+} ions emission*

In order to investigate the dispersion of Yb^{3+} ions in the glass matrix, the luminescence decay curves of ytterbium $^{2}F_{5/2}$ excited state was measured for the PZn:Ag-0.25 Yb, PZn:Ag-2Yb and PZn:Na-2Yb glasses and the excited state lifetimes values were determined by fitting the curves. The samples were excited at 940 nm and the emissions were collected at 1040 nm. Fig. 3 shows the time resolved data and the corresponding fitting curve for the PZn:Ag-2Yb glass. All sample exhibits similar decay curve profile. The fitting was successfully done using two exponential decay functions leading to two different time constants, a shorter one of around tens of microseconds and a longer one a few milliseconds. The short component is related to the characteristic

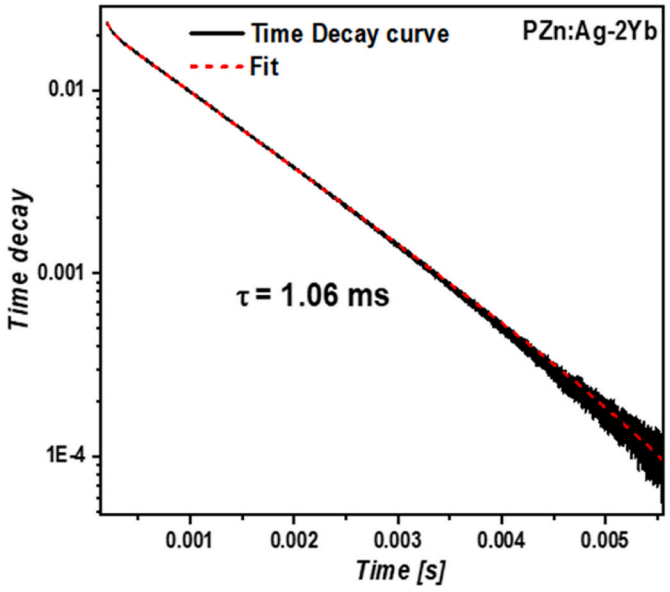

Fig. 3. Lifetime of Yb^{3+} in the PZn:Ag-2Yb glass (excitation at 940 nm).

response time of the instrument. The longest component is related to the Yb^{3+} ions decay time. The value are respectively 1.23 ms, 1.06 ms and 1.21 ms for PZn:Ag-0.25 Yb, PZn:Ag-2Yb and PZn:Na-2Yb glasses. Considering the intrinsic error of the measurements to be around 10%, one cannot observe a noticeable difference between the different samples. The collected data is in good agreement with the value previously reported for well dispersed Yb^{3+} ions in glass and crystalline compounds [20–23]. Those results give evidence that, up to this doping level, Yb^{3+} ions occupy a similar chemical environment in the different glass matrix and that they do not experience any clustering.

3.4. Femtosecond laser writing of fluorescent structures

Femtosecond laser writing has been investigated in both the Yb^{3+}-doped silver-containing PZn:Ag-0.25 Yb and PZn:Ag-2Yb, the writing in the Yb^{3+}-free PZn:Ag being largely reported elsewhere [2–5]. No specific laser-induced fluorescence contrast was observed in the PZn:Na-2Yb glass containing no silver ions, so such composition will not be considered anymore hereafter.

Femtosecond laser writing of the glasses has been performed 160 μm below the glass surface, being composed of several identical square patterns resulting from different laser irradiances and sample's velocity. Each square pattern is a 100 × 100 μm^2 structure with an interline spacing of 10 μm between successive laser passes. The structures were created by the linear translation of the glass sample with control speed motion of 10, 50, and 100 $\mu m.s^{-1}$ and different laser irradiances estimated between 5.83 and 8.93 $TW.cm^{-2}$. Such parameters are standard for activating the photochemistry of silver and associated fluorescent properties [2–5]. In this framework, Fig. 4 shows a wide-field fluorescence microscopy image of the laser-inscribed interaction matrix in the PZn:Ag-2Yb sample (imaging objective 10 × – NA 0.3, excitation at 375 nm, collection over the visible range). Square patterns were inscribed with decreasing speeds from 100 $\mu m.s^{-1}$ to 10 $\mu m.s^{-1}$ (thus increasing the cumulated laser pulses from 0.16 × 10^6 to 1.6 × 10^6 pulses, typically) from left to right, and with increasing laser peak irradiances from bottom to top. The onset shows a magnified image of a given pattern, highlighting the creation of a double-track material modification at the edge of the laser/matter interaction voxel, associated with the resulting pulse-to-pulse creation of highly fluorescent molecular silver clusters [2–5]. Indeed, as reported elsewhere, the interaction of the femtosecond laser pulse train with the silver ion (Ag^+) containing glass triggers silver-based photochemistry. First, free electrons and holes generated by

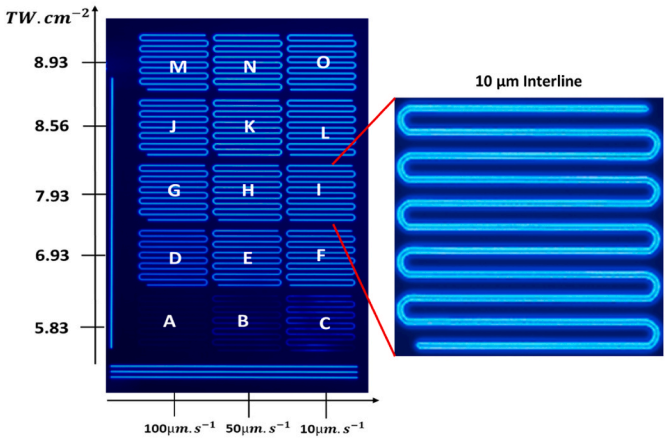

Fig. 4. Laser/glass interaction matrix showing luminescent square patterns versus laser peak irradiance and sample motion velocity (wide-field fluorescence micrograph under excitation at 375 nm, objective 10 × , NA 0.3. Onset: magnified pattern showing the typical double-track fluorescence profile along the laser pass.

the multi-absorption process are trapped by silver ions to form mobile silver atoms Ag^0 as well as hole-trapped centers Ag^{2+}. The high repetition rate irradiation (at 9.8 MHz) allows the pulse-after-pulse diffusion of Ag^0 which combines with the remaining Ag^+ to form the preliminary silver clusters Ag_2^+. Subsequently, such Ag_2^+ clusters keep on reacting with other mobile silver species, leading to the formation of larger silver clusters Ag_m^{x+} (with m <10 [24–26]) that exhibit high fluorescent emission in the visible range. The overall final aspect of the fluorescent double-track profile results from the final budget between the successive laser-induced creation and photodissociation of silver clusters, as well as the progressive consumption of the available silver elements in the central part of the laser beam [2–5]. As reported elsewhere, Fig. 4 illustrates that the creation of silver clusters and associated fluorescence intensity increases with the deposited dose during laser irradiation, both with the incident laser peak irradiance and with the cumulated number of pulses [2–5]. Although counter-intuitive, the involved process of silver cluster production corresponds to a regime with a very moderate temperature increase (up to a few tens of degrees), despite the high repetition rate regime [27]. Similarly to what was observed in the case of Eu^{3+}-doped silver-containing phosphate glass [4], the insertion of Yb^{3+} ions at the considered concentrations (Yb^{3+}-free, 0.25%, and 2% molar) did not significantly affect nor modify the laser inscription process based of the induced photochemistry of silver.

3.5. Femtosecond laser inscription of refractive index modifications

As reported by Abou Khalil et al. [28], the femtosecond laser inscription of silver clusters is accompanied by a local refractive index modification being exactly co-located with the silver cluster fluorescent patterns. Indeed, the creation of new silver molecules corresponds to the formation of new chemical bonds showing enhanced polarizability [28]. As a consequence, a positive refractive index modification is induced for light in the visible range by the silver cluster distributions, leading to structures that are compatible with waveguiding and evanescent sensors [28,29].

All the laser-inscribed patterns, such as those shown in Fig. 4, have been imaged by means of phase imaging microscopy using a wave-front sensor SID4Bio from PHASICS. Cross-sections of the laser passes have been extracted, as shown in Fig. 5. Indeed, Fig. 5(a) and (b) show the refractive index change (Δn) profile of the abovementioned square pattern labeled L (Fig. 4) written with 10 $\mu m.s^{-1}$ speed and 8.53 TW cm^{-2} laser irradiance, both in the 0.25% and 2% Yb^{3+}-doped PZn:Ag–Yb glasses. As reported in the DLW on zinc phosphate glass (PZn:Ag)

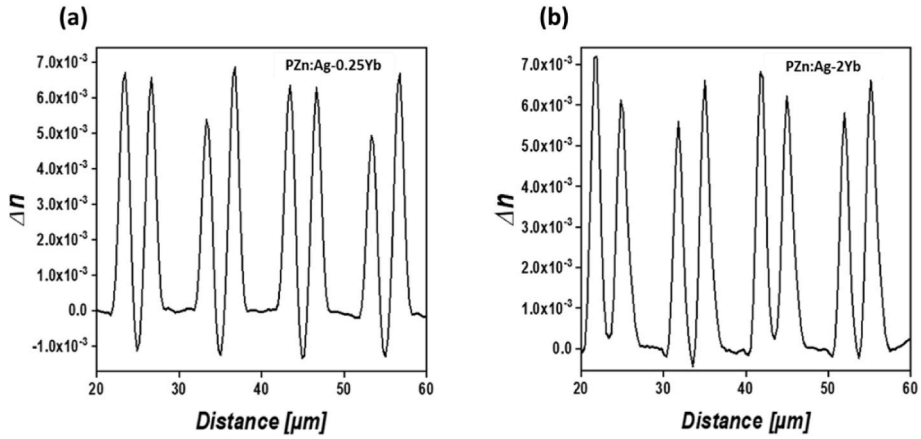

Fig. 5. Profile of the refrective index change of four laser inscription passes, depicting a positive double-track distribution (up to 7 × 10^{-3}) perfectly co-located to that of the laser-induced silver clusters, as shown by the onset of Fig. 4. (a, b) PZn:Ag-0.25 and PZn:Ag-2Yb samples, respectively.

[28–30], the positive Δn corresponds to the spatial distribution of silver clusters, so that each laser pass induces a positive double-track Δn profile, perfectly correlated to the fluorescent double-track profile related to the distribution of laser-induced silver clusters. This can be correlated to the positive double-track Δn profile in the two samples PZn:Ag-0.25 Yb and PZn:Ag-2Yb showing high values up to 7 × 10^{-3}, which is similar to what was observed by Abou Khalil et al., in PZn:Ag glass matrix with equivalent silver concentration [28]. The negative Δn contribution at the center of each laser pass, namely between the positive double-track Δn profile, is associated with the decrease of the Ag^{+} ion concentration at the center of the interaction voxel, partially leading to a decrease of the local density and polarizability of the glass matrix [28]. Such negative contribution (slightly more pronounced here in the 0.25% Yb^{3+}-doped sample) remains minor compared to the surrounded positive double-track Δn profile so that waveguiding and integrated photonic applications are possible [28,29].

Laser/glass interaction matrix have been systematically exploited, by extracting the positive double-track Δn amplitude versus laser irradiation parameters. For each pattern of the interaction matrix in the PZn: Ag-0.25 Yb and PZn:Ag-2Yb glasses, the positive Δn averaged amplitudes and associated standard deviations have been determined by considering the profiles of eight double-track profiles resulting from four laser passes, as shown by Fig. 6. Because, the Δn modification is supported by the creation of silver clusters, the behavior of the refractive index modifications typically follows that of laser-inscribed fluorescence features, both in terms of spatial distribution and of amplitude evolution with laser irradiation conditions. Indeed, the Δn amplitude increases with laser irradiance, similarly for both PZn:Ag-0.25 Yb and PZn:Ag-2Yb glasses, corroborating that the Yb^{3+} ion insertion does not significantly affect the mechanisms at play during the laser writing involving silver photochemistry, at least at such concentration doping levels. As shown in Fig. 6, the refractive index modification Δn for both glasses increases with laser irradiance, revealing a saturation behavior for the largest irradiances. The Δn increase is more efficient for the largest deposited dose, namely for the lowest sample velocities leading to the highest cumulated numbers of pulses. However, the Δn dependence also shows a saturation behavior with the cumulated numbers of pulses, as visible with Δn values less than 10 times larger for the 10 μm.s^{-1} and 100 μm.s^{-1} velocity conditions. This trend was quite similar to what was proposed by Abou Khalil et al., in PZn:Ag glass [28], It is also noticed that the threshold of DLW with Ag and Yb-containing glass may be slightly above that of purely Ag-containing glass. This may be mentioned that a minor part of energy deposition might be used to direct multi-photon excitation of the charge transfer band of Yb3+ so that slightly less intensity is available for Ag excitation. Such a competitive effect on energy deposition processes leads to a slight increase in DLW threshold with silver:

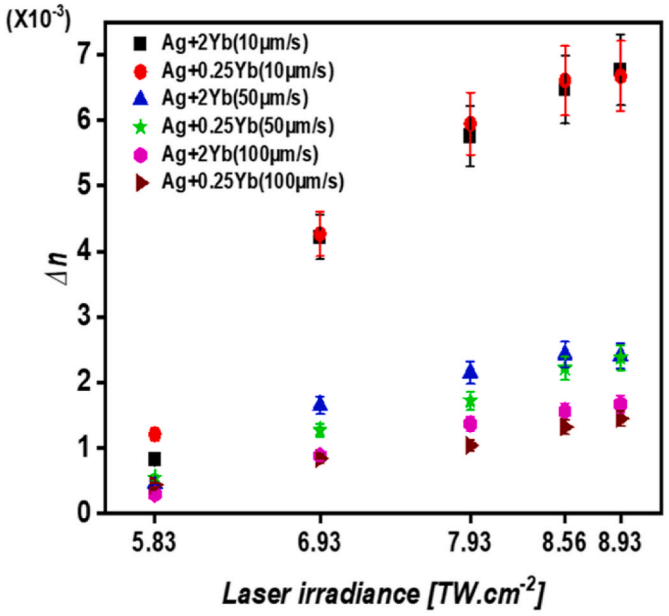

Fig. 6. Amplitude of the positive refractive index modification Δn versus laser irradiance, for different velocities and associated a cumulated number of pulse, for both the PZn:Ag-0.25 and PZn:Ag-2Yb glasses, showing the increase and progressive saturation behavior of such Δn modification with the deposited dose by laser irradiation.

from slightly above 5 TW.cm^{-2} [28] up to slightly less than 5.8 TW.cm^{-2}.

The behavior of the Δn modification follows that of the laser-induced creation of silver clusters, similarly to what was modeled in detail by Smetanina et al. where the multi-photon energy deposition, the mobile species diffusion, and chemical reactivity, as well as the pulse-after-pulse management of the silver ion reservoir, had been taken into account [27]. Desmoulin et al. had indeed directly observed by means of a chemical micro-probe the depletion of silver elements at the center of laser irradiation, confirming the overall pulse-after-pulse diffusion of silver elements [31]. Recently, Loi et al. extended the evidence of the preponderant role of the management of silver ion reservoir, by addressing the influence of successive multi-passes on the Δn amplitude, reaching remarkable values up to 2 × 10^{-2} in a silver-containing commercial glass [32]. On the one hand, these reported results corroborate the interpretation of saturation of the laser inscription process (both silver cluster formation, fluorescence emission, and correlative refractive index modification) with the cumulated number of pulses, by means

of depletion of the available silver ion reservoir. On the other hand, the saturation of the laser inscription process with laser irradiance (for a large enough number of pulses) is to be understood in a slightly different manner than that of the strict availability of the silver ion reservoir. Indeed, the pioneering work of Bellec et al. had shown that the efficiency of laser inscription of fluorescent silver clusters was highly dependent on the laser repetition rate [33]. The induced fluorescence was following a strong drop while reducing the laser repetition rate by decades, from the 10 MHz range down to the 100 kHz range, for given laser irradiances and fixed cumulated numbers of pulses, whatever the considered repetition rate. This demonstrates that the considered laser inscription mechanism includes a pulse-to-pulse memory effect so that the contribution of each laser pulse is highly dependent on the transient material state that results from the previous laser pulse. Thus, the transient species such as hole trap centers (Ag^{2+}) and electrons trap centers (Ag^{0}) remaining from the laser pulse #N-1 interact with the free photoelectrons produced by multi-photon absorption by the laser pulse #N, leading to the pulse-after-pulse formation of new silver clusters. As a consequence, the Δn saturation in Fig. 6 with the laser irradiance can be understood as the saturation of the remaining transient species produced by the laser pulse #N-1, which limits the pulse-to-pulse efficiency of the following pulse #N. The proposed interpretation of silver cluster production and associated saturation behaviors appear to equally stand for both Yb^{3+}-free and Yb^{3+}-doped silver-containing glasses.

3.6. *Confocal luminescence of Yb^{3+} ions at the laser-induced fluorescence patterns*

The influence of laser inscription of highly-localized fluorescent silver clusters on the fluorescence emission of Yb^{3+} ions was also investigated. Fig. 7(a–c) show the micro-emission spectra measured at the laser-induced patterns for the 10 μm.s^{-1} sample velocity and distinct laser irradiances. The patterns were excited at three different excitation wavelengths (325 nm, 405 nm, and 532 nm).

As reported elsewhere, the emission spectrum related to the photo-induced silver clusters shows a broadband emission that lies in the visible, with a usual relative Stokes shift when considering excitation radiations with increasing wavelengths from 325 nm, 405 nm to 532 nm [4]. The emission spectrum of silver clusters encompasses the whole visible range with a maximum of around 525 nm when excited in the UV range [2–5]. Such silver cluster emission increases with the laser-deposited dose, namely with the laser irradiance and the cumulated number of pulses [2–5]. It is noticeable in Fig. 7 that the emission of Yb^{3+} ions co-located at the silver cluster patterns shows the same dependence with laser irradiation parameters as that of the silver cluster fluorescence (as previously shown in Fig. 4).

For excitation at 325 nm, an increasing enhancement of the Yb^{3+} emission intensity is observed with the laser inscription irradiance (patterns C to O), comparatively to the emission of the pristine glass (Fig. 7a). The increase of the laser irradiance at the given sample's velocity promotes the more efficient formation of silver clusters, which is correlated to the enhancement of the co-located Yb^{3+} emission. This indicates the strong influence of the number of silver clusters in the vicinity of the Yb^{3+} ions. Note that the pristine glass emission is non-zero, as previously shown by the Yb^{3+} excitation spectrum in Fig. 2d. For excitation at the longer wavelength of 405 nm, the Yb^{3+} emission follows a similar enhancement with the laser inscription irradiance to what was observed for the 325 nm excitation (Fig. 7b). However, the relative amplitude of the Yb^{3+} emission of the pristine glass appears weaker, in agreement with the decrease of the excitation spectrum of Yb^{3+} from 325 nm to 405 nm, as shown in Fig. 2d. However, for excitation at 532 nm, Yb^{3+} ions cannot be excited so that the near-IR emission of the pristine glass becomes null and the laser-inscribed patterns show a remarkable background-free emission. As a consequence, the 532 nm excitation promotes the Yb^{3+} emission only mediated through the laser-inscribed patterns (Fig. 7c). This suggests the ability to activate a near-IR emission of the Yb^{3+} ions being fully mediated by the excited silver clusters, thanks to the occurrence of efficient non-radiative

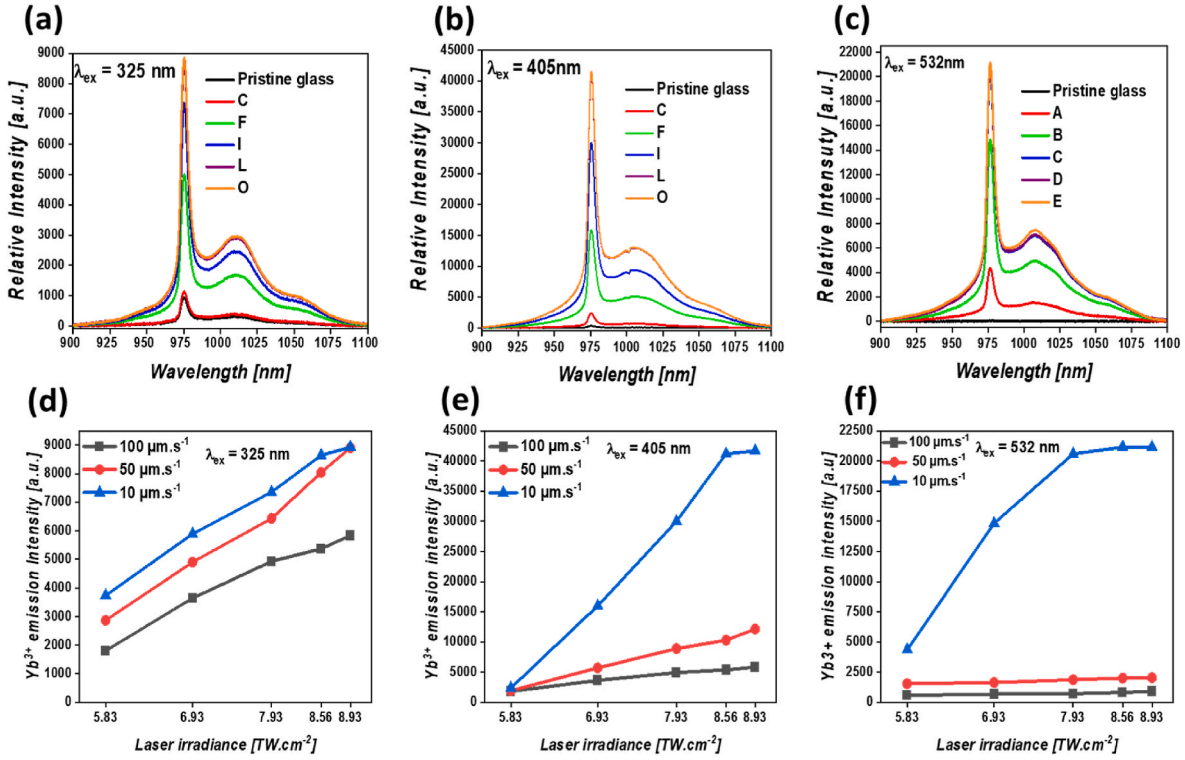

Fig. 7. (a, b, c) Confocal near-IR fluorescence emission spectra of the PZn:Ag-2Yb sample from the laser-created patterns inscribed at 10 μm.s^{-1} from Fig. 2, for excitation wavelengths at 325 nm, 405 nm, and 532 nm, respectively. (d, e, f) Associated zero-phonon line amplitudes spectra of the Yb^{3+} ions for all the patterns of the interaction matrix from Fig. 2.

energy transfer from the silver clusters to Yb^{3+}. In such a condition of excitation of the silver clusters out of the direct excitation range of the Yb^{3+} ions, the excitation of the latter appears as completely indirect, allowing for the creation of background-free near-IR emitting structures. One can also observe a slight modification in the spectra shape for the three excitations wavelength, which is probably due to the instrumentation defect and the use of different filters for excitation rejection during the emission data collection.

Every pattern of the laser/glass interaction matrix for the PZn:Ag-2Yb sample iluustrated in Fig. 4 has been investigated by extracting the peak amplitude of the zero-phonon line at 976 nm of the Yb^{3+} emission, as shown in Fig. 7(a–c) for the three considered excitation wavelengths at 325 nm, 405 nm, and 532 nm, respectively.

Fig. 7(d) shows that, when excited at 325 nm, the Yb^{3+} emission intensity with laser irradiance is moderately dependent on the sample's velocity during the irradiation process. For excitation at 405 nm, the sample's velocity plays a larger role, showing a significantly reduced enhancement of the Yb^{3+} emission for a lower cumulated number of pulses related to the faster sample's velocity (50 $\mu m.s^{-1}$ and 100 $\mu m.s^{-1}$, compared to the 10 $\mu m.s^{-1}$ velocity), as shown in Fig. 7e. Moreover, such a dose-dependent effect is even more pronounced for the 532 nm excitation. Indeed, the enhancement of the Yb^{3+} emission intensity with the laser irradiance is observed to be mostly limited to patterns inscribed at the 10 $\mu m.s^{-1}$ velocity, while faster velocities tend to show no such a near-IR emission and enhancement (Fig. 7f). Considering that the laser inscription regime of silver clusters is very gentle to the glass matrix itself [27], the initial distribution of Yb^{3+} ions is assumed not to be affected by the laser inscription process, so the Yb^{3+} ions are considered not to move due to their size and charge. In parallel, several populations of distinct silver clusters happen to be formed during the inscription process depending on the irradiation velocity [25], each family of clusters exhibits different excitation bands from UV to visible. The 325 nm excitation promotes the excitation of all silver cluster's families, without giving access to any selectivity among these cluster families concerning the resonant energy transfers towards the Yb^{3+} ions. However, while considering excitations at higher wavelengths, one preferentially promotes the excitation of the cluster's family having an excitation band tail in the visible range, leading to existing resonant energy transfers all from the excited clusters. Such clusters appear thus to require a large cumulated number of pulses to be generated, being mostly formed at the 10 $\mu m.s^{-1}$ velocity. As a consequence, the observation of energy transfer efficiency evolutions with laser irradiation parameters and with excitation wavelengths happens to be a relevant approach to indirectly reveal the existence of distinct families of clusters with distinct population concentrations, although it is still difficult to determine the explicit nature and concentration of such cluster families. In this framework, the presence of the Yb^{3+} ions acts as a local probe to indirectly reveal the existence of families of clusters, while the observation of such diversity is in agreement with both reported theoretical and experimental investigations [4]. The final noticeable aspect is that resonant energy transfers also give an indirect experimental visualization of the mentioned saturation of silver cluster production with the laser irradiation parameters (laser irradiance and a cumulated number of pulses) during the laser inscription process, as detailed in Section 3.4. Indeed, this can be observed by the correlated saturation of the efficiency of the resonant energy transfer, as shown with the saturation of the near-IR Yb^{3+} emission for the largest laser irradiations and cumulated number of pulses, especially observable for an inscription at 10 $\mu m.s^{-1}$ while excited at 405 nm and even more at 532 nm.

The highly-localized creation of silver clusters on the one hand, and the resulting resonant energy transfers towards Yb^{3+} ions, on the other hand, provide an elegant manner to generate highly-localized near-IR fluorescent emission patterns with sub-diffraction features, despite the fact that such near-IR emitters are randomly distributed all over the glass material. Beyond the local property of spatially-selective background-free excitation of the Yb^{3+} ions, one can thus create multi-scale fluorescent architectures with concomitant background-free visible and near-IR emission. This is illustrated by Fig. 8, showing the laser inscription of a planar pattern that corresponds to a fluorescent target. Thanks to the sub-micron scale laser inscription for silver clusters on the one hand, and the associated resonant energy transfers to Yb^{3+} ions, on the other hand, such a high-resolution pattern shows sub-diffraction features compatible with the creation of fluorescent optical standards for advanced confocal microscopy encompassing both the visible and near-IR spectral range (Fig. 8(a) and (b), respectively). Such photonic architectures can also play a role in near-IR display devices and/or in fraud analysis with counter-faint marking approaches.

4. Conclusion

The ability to develop glass matrix exhibiting good photosensitivity with 3D local luminescence features from UV to the near-infrared range was proven. Zinc phosphate glasses containing silver and Yb^{3+} were demonstrated as good candidates to produce such luminescence features. Photoluminescence characterization of the as-prepared glasses revealed that silver and Yb^{3+} ions are homogeneously distributed with no cluster formation. For the glass containing silver and Yb^{3+}, the presence of Yb^{3+} slightly influences the distribution of silvers ions in two different sites. The enhancement of Yb^{3+} emission in the silver-containing Yb^{3+} glass compared to the silver-free glass highlights the phenomenon of energy transfer from silver ions to rare earth ions. Femtosecond direct laser writing shows the ability to induce 3D localized fluorescent structure based on the photochemistry of silver ions by the formation of silver clusters without apparent influences of Yb^{3+} ions content in the inscription process. The micro-luminescence spectroscopy measurements performed on the DLW patterns allowed the demonstration that the enhancement of Yb^{3+} emission is co-localized with the laser inscribed fluorescent silver cluster. An efficient resonant energy transfer from silver clusters to the Yb^{3+} ions has been proposed. The results show the ability to create 3D fluorescent patterns exhibiting both luminescent properties in the visible originating from the silver cluster and in the near-infrared range originating from the co-localized Yb^{3+} ions, as well as a local modification of the refractive index. This finding highly supports the energy transfer phenomena of the silver cluster to other rare earth such as Eu^{3+} published elsewhere [4] and can be at the origin of the creation of new photonic architecture with applications in the near-infrared range.

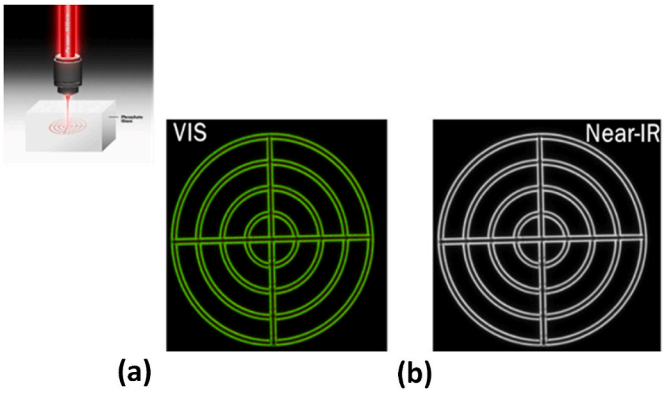

Fig. 8. Confocal image of a multi-scale photonic architecture showing sub-diffraction features, corresponding to a fluorescent target for high-resolution calibration optical standard for confocal fluorescence microscopy, for excitation at 473 nm. (a) Emission of the silver clusters integrated into the visible range over the 500–700 nm range; (b) co-localized near-IR emission of the Yb^{3+} ions integrated over the 920–1050 nm range. Scale: concentric circles show radii with a 5 μm increment.

Funding

This research has benefited from financial support from French National Research Agency (ANR) ANR-19-CE08-0021-01, and from Région Nouvelle Aquitaine (project AAPR2020-2019-8193110). This project has received support funding from GPR IDEX Bordeaux and French National Research Agency (ANR) ANR- 21-PRRD-0001-01/PDR- Stabilo. The Brazilian team would like to acknowledge funding from FAPESP – *Fundação de Amparo a Pesquisa do Estado de São Paulo*, through the CeRTEV project N. 2013/07793-6. GG is personally grateful to FAPESP for the Postdoctoral scholarship N. 2018/03931-9.

Institutional review board statement

Not applicable.

Informed consent statement

Not applicable.

CRediT authorship contribution statement

Fouad Alassani: Conceptualization, Data curation, Investigation, Methodology, Writing – original draft. **Gustavo Galleani:** Investigation. **Guillaume Raffy:** Investigation, Writing – review & editing. **André Del Guerzo:** Writing – review & editing. **Arnaud Royon:** Funding acquisition, Investigation. **Kevin Bourhis:** Funding acquisition, Investigation. **Andrea Simone Stucchi de Camargo:** Funding acquisition, Writing – review & editing. **Véronique Jubera:** Writing – review & editing. **Lionel Canioni:** Funding acquisition, Supervision. **Thierry Cardinal:** Conceptualization, Funding acquisition, Methodology, Resources, Supervision, Validation, Writing – review & editing. **Yannick Petit:** Conceptualization, Funding acquisition, Methodology, Resources, Supervision, Investigation, Validation, Writing – review & editing.

Declaration of competing interest

The authors declare that they have no known competing financial interests or personal relationships that could have appeared to influence the work reported in this paper.

Data availability

No data was used for the research described in the article.

Acknowledgments

Not applicable.

References

[1] S. Gross, , et al.M.J. Withford, « Ultrafast-laser-inscribed 3D integrated photonics: challenges and emerging applications », Nanophotonics 4 (3) (nov. 2015) 332–352, https://doi.org/10.1515/nanoph-2015-0020.

[2] A. Royon, K. Bourhis, M. Bellec, G. Papon, B. Bousquet, Y. Deshayes, T. Cardinal, L. Canioni, « silver clusters embedded in glass as a perennial high capacity optical recording medium », Adv. Mater. 22 (46) (2010) 5282–5286, https://doi.org/10.1002/adma.201002413.

[3] K. Bourhis, A. Royon, M. Bellec, J. Choi, A. Fargues, M. Treguer, J.-J. Videau, D. Talaga, M. Richardson, T. Cardinal, L. Canioni, Femtosecond laser structuring and optical properties of a silver and zinc phosphate glass, J. Non-Cryst. Solids 356 (44) (oct. 2010) 2658–2665, https://doi.org/10.1016/j.jnoncrysol.2010.03.033.

[4] Y. Petit, G. Galleani, G. Raffy, J.-C. Desmoulin, V. Jubéra, A. Guerzo, A.S.S. de Camargo, L. Canioni, T. Cardinal, « three-dimensional high spatial localization of efficient resonant energy transfer from laser-assisted precipitated silver clusters to trivalent europium ions », Crystals 11 (2) (févr. 2021) https://doi.org/10.3390/cryst11020148. Art. n° 2.

[5] Y. Petit, S. Danto, T. Guérineau, A.A. Khalil, A. Le Camus, E. Fargin, G. Duchateau, J.-P. Bérubé, R. Vallée, Y. Messaddeq, T. Cardinal, L. Canioni, « on the femtosecond laser-induced photochemistry in silver-containing oxide glasses: mechanisms, related optical and physico-chemical properties, and technological applications », Adv. Opt. Technol. 7 (5) (oct. 2018) 291–309, https://doi.org/10.1515/aot-2018-0037.

[6] R. Ma, J. Qian, S. Cui, X. Qiao, F. Wang, , et al.X. Fan, « Enhancing NIR emission of Yb^{3+} by silver nanoclusters in oxyfluoride glass », J. Lumin. 152 (2014) 222–225, https://doi.org/10.1016/j.jlumin.2013.10.036.

[7] R. Ma, J. Gao, Q. Xu, S. Cui, X. Qiao, J. Du, X. Fan, « Eu^{2+} promoted formation of molecule-like Ag and enhanced white luminescence of Ag/Eu-codoped oxyfluoride glasses », J. Non-Cryst. Solids 432 (janv. 2016) 348–353, https://doi.org/10.1016/j.jnoncrysol.2015.10.032.

[8] Z. Guo, S. Ye, T. Liu, S. Li, , et al.D. Wang, « SmF3 doping and heat treatment manipulated Ag species evaluation and efficient energy transfer from Ag nanoclusters to Sm3+ ions in oxyfluoride glass », J. Non-Cryst. Solids 458 (févr. 2017) 80–85, https://doi.org/10.1016/j.jnoncrysol.2016.11.026.

[9] Y. Shi, S. Ye, J. Yu, H. Liao, J. Liu, , et al.D. Wang, « Simultaneous energy transfer from molecular-like silver nanoclusters to Sm^{3+}/Ln^{3+} (Ln = Eu or Tb) in glass under UV excitation », Opt Express 27 (26) (déc. 2019) 38159–38167, https://doi.org/10.1364/OE.380860.

[10] O.L. Malta, P.A. Santa-Cruz, G.F. De Sá, , et al.F. Auzel, « Fluorescence enhancement induced by the presence of small silver particles in Eu3+ doped materials », J. Lumin. 33 (3) (mai 1985) 261–272, https://doi.org/10.1016/0022-2313(85)90003-1.

[11] H. Liao, S. Ye, R. Shen, X. Li, , et al.D. Wang, « Effective formation of Ag nanoclusters and efficient energy transfer to Yb^{3+} ions in borosilicate glasses for photovoltaic application », Mater. Res. Bull. 111 (mars 2019) 113–117, https://doi.org/10.1016/j.materresbull.2018.10.042.

[12] H. Lin, D. Chen, Y. Yu, R. Zhang, , et al.Y. Wang, « Molecular-like Ag clusters sensitized near-infrared down-conversion luminescence in oxyfluoride glasses for broadband spectral modification », Appl. Phys. Lett. 103 (9) (août 2013), 091902 https://doi.org/10.1063/1.4819951.

[13] J.A. Jiménez, S. Lysenko, H. Liu, , et al.M. Sendova, « Luminescence of trivalent samarium ions in silver and tin co-doped aluminophosphate glass », Opt. Mater. 33 (8) (juin 2011) 1215–1220, https://doi.org/10.1016/j.optmat.2011.02.013.

[14] M. Eichelbaum, , et al.K. Rademann, « plasmonic enhancement or energy transfer? On the luminescence of gold-, silver-, and lanthanide-doped silicate glasses and its potential for light-emitting devices », Adv. Funct. Mater. 19 (13) (2009) 2045–2052, https://doi.org/10.1002/adfm.200801892.

[15] J.R. Lakowicz, « Radiative decay engineering 5: metal-enhanced fluorescence and plasmon emission », Anal. Biochem. 337 (2) (févr. 2005) 171–194, https://doi.org/10.1016/j.ab.2004.11.026.

[16] C. Maurel, T. Cardinal, M. Bellec, L. Canioni, B. Bousquet, M. Treguer, J.J. Videau, J. Choi, M. Richardson, « Luminescence properties of silver zinc phosphate glasses following different irradiations », J. Lumin. 129 (12) (déc. 2009) 1514–1518, https://doi.org/10.1016/j.jlumin.2008.12.023.

[17] K.M. Davis, A. Agarwal, M. Tomozawa, , et al.K. Hirao, « Quantitative infrared spectroscopic measurement of hydroxyl concentrations in silica glass », J. Non-Cryst. Solids 203 (août 1996) 27–36, https://doi.org/10.1016/0022-3093(96)00330-4.

[18] M.J.V. Bell, W.G. Quirino, S.L. Oliveira, D.F.D. Sousa, , et al.L.a.O. Nunes, « Cooperative luminescence in Yb^{3+}-doped phosphate glasses », J. Phys. Condens. Matter 15 (27) (2003). Art. n° 27.

[19] V.K. Tikhomirov, T. Vosch, E. Fron, V.D. Rodríguez, J.J. Velázquez, D. Kirilenko, G. Van Tendeloo, J. Hofkens, M. Van der Auweraer, V.V. Moshchalkov, « Luminescence of oxyfluoride glasses co-doped with Ag nanoclusters and Yb3+ ions », RSC Adv. 2 (4) (janv. 2012) 1496–1501, https://doi.org/10.1039/C1RA01026C.

[20] J.M. Ward, D.G. O'Shea, B.J. Shortt, , et al.S.N. Chormaic, « Optical bistability in Er-Yb codoped phosphate glass microspheres at room temperature », J. Appl. Phys. 102 (2) (juill. 2007), 023104 https://doi.org/10.1063/1.2753591.

[21] L. Wang, H. Zeng, B. Yang, F. Ye1, J. Chen, G. Chen1, A.T. Smith, L. Sun, « structure-dependent spectroscopic properties of Yb^{3+}-doped phosphosilicate glasses modified by SiO2 », Materials 10 (3) (mars 2017) https://doi.org/10.3390/ma10030241. Art. n° 3.

[22] V. Jubera, J. Sablayrolles, F. Guillen, R. Decourt, M. Couzi, , et al.A. Garcia, « from the infrared to the visible range: spectroscopic studies of ytterbium doped oxyborates », Opt Commun. 282 (1) (2009) 53–59, https://doi.org/10.1016/j.optcom.2008.09.075.

[23] J. Sablayrolles, V. Jubera, F. Guillen, R. Decourt, M. Couzi, J.P. Chaminade, A. Garcia, « Infrared and visible spectroscopic studies of the ytterbium doped borate Li6Y(BO3)3 », Opt Commun. 280 (1) (déc. 2007) 103–109, https://doi.org/10.1016/j.optcom.2007.07.034.

[24] B.G. Ershov, E. Janata, , et al.A. Henglein, « Growth of silver particles in aqueous solution: long-lived "magic" clusters and ionic strength effects », J. Phys. Chem. 97 (2) (janv. 1993) 339–343, https://doi.org/10.1021/j100104a013.

[25] N. Marquestaut, Y. Petit, A. Royon, P. Mounaix, T. Cardinal, , et al.L. Canioni, « three-dimensional silver nanoparticle formation using femtosecond laser irradiation in phosphate glasses: analogy with photography », Adv. Funct. Mater. 24 (37) (2014) 5824–5832, https://doi.org/10.1002/adfm.201401103.

[26] R. Espiau de Lamaestre, H. Béa, H. Bernas, J. Belloni, , et al.J.L. Marignier, « Irradiation-induced Ag nanocluster nucleation in silicate glasses: analogy with photography », Phys. Rev. B 76 (20) (nov. 2007), 205431 https://doi.org/10.1103/PhysRevB.76.205431.

[27] E. Smetanina, B. Chimier, Y. Petit, N. Varkentina, E. Fargin, L. Hirsch, T. Cardinal, L. Canioni, G. Duchateau, « Modeling of cluster organization in metal-doped oxide glasses irradiated by a train of femtosecond laser pulses », Phys. Rev. A 93 (1) (janv. 2016), 013846 https://doi.org/10.1103/PhysRevA.93.013846.

[28] A.A. Khalil1, J.-P. Bérubé, S. Danto, J.-C. Desmoulin, T. Cardinal, Y. Petit, R. Vallée, L. Canioni, « Direct laser writing of a new type of waveguides in silver containing glasses », Sci. Rep. 7 (1) (sept. 2017) https://doi.org/10.1038/s41598-017-11550-0. Art. n° 1.

[29] A.A. Khalil, J.-P. Bérubé, S. Danto, T. Cardinal, Y. Petit, R. Vallée, L. Canioni, « Comparative study between the standard type I and the type A femtosecond laser induced refractive index change in silver containing glasses », Opt. Mater. Express 9 (6) (juin 2019) 2640–2651, https://doi.org/10.1364/OME.9.002640.

[30] A.A. Khalil, P. Lalanne, J.-P. Bérubé, Y. Petit, R. Vallée, L. Canioni, « Femtosecond laser writing of near-surface waveguides for refractive-index sensing », Opt Express 27 (22) (oct. 2019) 31130–31143, https://doi.org/10.1364/OE.27.031130.

[31] J.-C. Desmoulin, Y. Petit, L. Canioni, M. Dussauze, M. Lahaye, H.M. Gonzalez, E. Brasselet, T. Cardinal, « Femtosecond laser structuring of silver-containing glass: silver redistribution, selective etching, and surface topology engineering », J. Appl. Phys. 118 (déc. 2015), 213104 https://doi.org/10.1063/1.4936233.

[32] L. Loi, Y. Petit, Y. Petit, , et al.L. Canioni, « High refractive index change in Type A laser modification using a multi-scan approach », Opt. Mater. Express 12 (6) (juin 2022) 2297–2308, https://doi.org/10.1364/OME.457655.

[33] M. Bellec, A. Royon, K. Bourhis, J. Choi, B. Bousquet, M. Treguer, T. Cardinal, J.-J. Videau, M. Richardson, L. Canioni1, « 3D patterning at the nanoscale of fluorescent emitters in glass », J. Phys. Chem. C 114 (37) (sept. 2010) 15584–15588, https://doi.org/10.1021/jp104049e.